NUCL SCI TECH (2019) 30:67
https://doi.org/10.1007/s41365-019-0592-4

Non-equilibrium ignition criterion for magnetized deuterium–tritium fuel

E. Ghorbanpour[1] · A. Ghasemizad[1] · S. Khoshbinfar[1]

Received: 19 March 2018 / Revised: 25 August 2018 / Accepted: 6 September 2018 / Published online: 23 March 2019

Abstract In this paper, non-equilibrium ignition conditions for magnetized cylindrical deuterium–tritium plasma in the presence of an axial magnetic field have been investigated. It is expected that temperature imbalance between ions and electrons as well as the axial magnetic field will relax the threshold of ignition conditions. Therefore, ignition conditions for this model are derived numerically involving the energy balance equation at the stagnation point. It has been derived using parametric space including electron and ion temperature (T_e, T_i), areal density (ρR), and seed magnetic field-dependent free parameters of B/ρ, mB, and BR. For $B/\rho < 10^6$ G cm^3 g^{-1}, $mB < 4 \times 10^4$ G cm g^{-1}, and $BR < 3 \times 10^5$ G cm, the minimum fuel areal density exceeds between $\rho R >$ 0.002 g cm^{-2}, $\rho R >$ 0.25 g cm^{-2}, and $\rho R >$ 0.02 g cm^{-2}, respectively. The practical equilibrium conditions also addressed which is in good agreement with the corresponding one-temperature magnetized mode proposed in previous studies. Moreover, it has been shown that the typical criterion of $BR \geq$ (6.13–4.64) $\times$ 10^5 G cm would be expectable. It is also confirmed that the minimum product of areal density times fuel temperature in equilibrium model is located in the range of T = 6–8 keV for all these free parameters, depending on the magnitude of the magnetic field. This is the entry point for the non-equilibrium model consistent with equilibrium model.

Keywords Magnetized plasma · Two-temperature model · Ion–electron non-equilibrium · Axial magnetic field · Ignition criteria

List of symbols

ρ	Mass density (g cm^{-3})
$R \equiv R_{stag}$	Cylinder radius at stagnation (cm)
n	Number density (cm^{-3})
n_e	Electron number density (cm^{-3})
n_i	Ion number density (cm^{-3})
n_D	Deuteron density (cm^{-3})
n_T	Triton density (cm^{-3})
T_e	Electron temperature (keV)
T_i	Ion temperature (keV)
B	Magnetic field (G)
v_0	Birth velocity of alpha particle (cm s^{-1})
ω_e	Electron cyclotron frequency (s^{-1})
ω_α	Larmor frequency of alpha particle (s^{-1})
ω_i	Ion cyclotron frequency (s^{-1})
c	Speed of light (cm s^{-1})
e	Unit charge (statC)
m_e	Electron mass (g)
m_i	Ion mass (g)
m_α	Alpha mass (g)
Z	Atomic number (-)
Z_α	Alpha atomic number (-)
E_f	Fusion energy (erg)
E_α	Alpha particle energy (erg)
E_n	Neutron energy (erg)
f_α	Fraction of alpha energy deposition (none)
l_α	Mean free path of alpha particle (cm)
$r_{\alpha L}$	Larmor radius of alpha particle (cm)
$\bar{R}$	Ratio of cylinder radius to mean free path of alpha particle (none)

✉ E. Ghorbanpour
eghorbanpour@phd.guilan.ac.ir;
e.ghorbanpour.t@gmail.com

1 Department of Physics, Faculty of Science, University of Guilan, P.O. Box 41335-1914, Rasht, Iran

b	Ratio of cylinder radius to Larmor radius of alpha particle (none)
k_B	Boltzmann constant (erg keV^{-1})
W_α	Fusion power density (erg cm^{-3} s^{-1})
$W_{\alpha,DT}$	DT fusion power density (erg cm^{-3} s^{-1})
$<\sigma v>_{DT}$	DT averaged reactivity (cm^3 s^{-1})
W_{br}	Bremsstrahlung power density (erg cm^{-3} s^{-1})
W_{hc}	Heat conduction power density loss (erg cm^{-3} s^{-1})
h	Planck constant (erg s)
κ_e	Braginskii thermal conductivity for electrons (cm^{-1} s^{-1})
κ_i	Braginskii thermal conductivity for ions (cm^{-1} s^{-1})
τ	Collision time (s)

1 Introduction

Magnetized target fusion (MTF) is known as a hybrid approach between two common fusion methods, i.e., inertial confinement fusion (ICF) and magnetic confinement fusion (MCF) [1–5]. MTF was coined by Lindemuth, and it is described as a method which deploys a liner/pusher implosion system to compress magnetized plasma to achieve thermonuclear fusion [6]. A magnetized target concept was separately conducted in Russia and the USA under the titles of MAGO (MAGnitnoye Obzhatiye, or magnetic compression) and MTF. Each one consists of a magnetized fuel and preheated confined plasma in the fusion target driven by an ion beam or laser pulse [7–9]. It is a combination of a standard ICF method with the applied seed magnetic field. The axial seed magnetic field on magnetized liner inertial fusion (MagLIF) at Sandia National Laboratory is approximately B_0 = 10–15 T where it is compressed to a high value of $B_z \geq$ 50-100 kT at stagnation [10, 11]. Reductions in radial thermal conduction losses due to electrons and ions of plasma as well as enhanced heating of alpha particles produced during the deuterium–tritium (DT) fusion reaction are examples of potential advantages of this proposal [12, 13]. Moreover, significant reductions in velocity requirements ($\sim 10^6$ cm s^{-1}), as well as hydrodynamics instability vulnerabilities in implosion stage, are quite expectable [14]. It implodes between sub-nanoseconds and hundreds of microseconds which results in an extension in the admissible values of ignition condition in a parameter space [15]. It also corresponds to a very low ρR parameter (areal density) of < 0.01 g cm^{-2}, up to high values of ~ 1.0 g cm^{-2} as happens in traditional ICF. The minimum areal density for non-magnetized cylindrical fuel, which is allowed to be ignited, is $\rho R \geq 0.45$ g cm^{-2} [16, 17]. Because of a considerable reduction in energy production costs, this novel approach to ICF earns enough attraction at economic scale, as well.

Widner proposed that applying a magnetic field to the fuel volume decreases thermal conduction, increases alpha energy deposition, and thus scales driver requirements down [18]. Magnetized fuel also relaxes high pressure values of ICF at the stagnation interval [19–21]. While ICF and MCF follow Lawson criterion in different pathways, MTF follows an intermediate choice; in fact, its goal is providing a plasma with densities around 10^{19} cm^{-3} located between ICF and MCF [22]. Leading research labs in the USA, such as Los Alamos National Laboratory (LANL), Sandia National Laboratories (SNL), OMEGA laser facility—Laboratory for Laser Energetics at the University of Rochester and Air Force Research Laboratory (AFRL), are the examples of currently working scientific groups on this approach [23]. Moreover, General Fusion in Canada is doing progressive experiments on MTF with a broad horizon by 2030. A novel magnetized target plasma design is working on spherically imploding plasma liners. The initial magnetic field is less than the cylindrical liners, i.e., $B_0 = 1.47 \times 10^3$ G–4.5×10^4 G with R_0 = 4–9.4 cm [24]. In spherical compression experiments on the OMEGA laser, the known application of magnetic field compression in plasma, relaxing ignition conditions for ICF, appears in the form of mean 15% increase in neutron-averaged ion temperature [25].

The main objective of this target design is to achieve the appropriate thermonuclear ignition and burn propagation at a much lower ignition condition. Traditionally, the ignition threshold can be determined by fuel temperature (T) and its areal density (ρR) characteristic parameters. The well-known ignition criterion for non-magnetized DT is T = 5–12 keV and $\rho R \geq$ 0.2–0.5 g cm^{-2}. In a magnetized case, ρR is no longer accounted as a reliable parameter for fuel ignition, and it is simply replaced by a BR parameter where B and R indicate the strength of seed magnetic field and fuel radius, respectively. So, the alternative ignition criterion is expressed by plasma temperature margins of T = 7–10 keV and $BR \geq (6.5\text{–}4.5) \times 10^5$ G cm in the framework of the equilibrium temperature model (i.e., $T_i = T_e$) [26, 27]. Ignition condition will reduce substantially if the imposed magnetic field is so strong to impede the escape of 3.5 MeV alpha particles. Consequently, the required driver power and expenses will decrease dramatically [28]. As the implosion velocities decrease in the MTF approach, the confinement times are extended which allow the efficient burn wave propagations. Generally, this provides hot spot ignition at lower ρR parameters. Hot spot ignition in ICF causes high energy gain by igniting the fuel from a small spark. Propagation of a burn wave into a fuel then results in burn. The hot volume is assumed to be tamped by a denser material, i.e., a tamper or dense fuel [29]. MagLIF simulations indicate that the areal density of ~ 0.07 g cm^{-2} of the DT layer is adequate for the beginning of burn wave propagation [30]. MagLIF evolution roadmap shows that by 2018 full DT performance will be achieved, and experiments at Z facility indicate that by stagnation and peak burn around 140 ns, the fuel has a radius $\rho R \sim 6$ mg cm^{-2} [10].

Magnetized targets are typically deigned either in spherical or cylindrical geometries [31]. Because of the inherent compatibility between the direction of beam illumination and target geometries, it is expected that the radial implosion of the fuel layer may be managed much easier in a cylindrical case [32]. A decade ago, the successful implementations of generating a hollow ion beam in the experiments were reported separately in the Institute for Theoretical and Experimental Physics within the framework of the ITEP TeraWatt Accumulator (TWAC) project and in the German Federal Research Institute for Heavy Ion Research (GSI) in the framework of the FAIR (Facility for Antiproton and Ion Research) project [33]. In laser-driven liner implosion of cylindrical targets, the laser beams are symmetrically illuminated on the cylinder wall [34]. In order to achieve the required field compression, the presence of the initial external magnetic field is obligatory.

In a simple ignition model, we may assume equal temperature for plasma components (i.e., electron and ion). However, in a realistic picture of fuel ignition, a non-equilibrium temperature model arises [35, 36]. Recent diagnostic studies of ignition condition in National Ignition Facility (NIF) targets reveal that hot spot parameters show more agreement with those values predicted by non-equilibrium temperature models, which can be observed in NIF ignition capsule implosions [34, 37]. Moreover, a non-equilibrium temperature model in a volume-ignited target shows that because the fuel may arrive in a temperature equilibrium mode at stagnation, it quickly transits to non-equilibrium ignition and burn phases. This transition mode improves energy yields and system performance [38]. In this model, it is suggested that electrons and ions have separate (T_e and T_i) temperatures. Ion–electron non-equilibrium relaxation is so efficient in such a way that it can expand ignition domain in ρR-T plane. Besides, one can provide situations in which this non- equilibrium condition persists in hot spot and sets up less ρR requirements to achieve self-heating [39].

In this paper, we present an analytic illustration of allowed ignition values of the areal densities of a magnetized DT fuel relevant to cylindrical geometry in the framework of the non-equilibrium two-temperature model. It is organized as follows: in Sect. 2, the mathematical and physical foundations of a non-equilibrium ignition model are presented which include the effective parameters in the energy balance equation, taking into account all the transport coefficients relevant to this geometry; and finally, in Sect. 3, the admissible values of fuel areal density at different physical situations are plotted and then analyzed. Moreover, a brief discussion on the consistency of the formalism and the expected values between equilibrium and non-equilibrium modes is presented.

2 Two-temperature model of magnetized DT fuel

In order to derive magnetized DT fuel ignition criterion in non-equilibrium temperature mode, i.e., $T_i \neq T_e$, we first discuss the parameters influenced by magnetic field. Noting the possibility of plasma having several temperatures, electrons and ions are often considered to have Maxwellian distribution with different T_e and T_i temperatures. This is due to the fact that the collision rate of electrons and ions with the same species is greater than their collision with a different one. Thus, although each species has its own thermal equilibrium, the plasma would have a non-equilibrium model. In the presence of a uniform magnetic field (B), plasma components possess their own cyclotron frequencies and follow different temperatures [40]. The variation of electron or ion temperature parallel or perpendicular to the magnetic field is neglected. Electron and ion cyclotron frequency in the magnetized DT fuel is obtained by [41]:

$$\omega_e\left[s^{-1}\right] = \frac{eB_0}{m_e c}, \quad \omega_i\left[s^{-1}\right] = \frac{ZeB_0}{m_i c}. \tag{1}$$

Considering the nuclear reaction of DT fuel to derive an energy balance equation, we have

$$d + t \rightarrow {}^4_2\mathrm{He}(3.5\ \mathrm{MeV}) + {}^1_0\mathrm{n}(14.1\ \mathrm{MeV}), \tag{2}$$

$$Q_{dt} = E_\alpha + E_n, \tag{3}$$

where E_α and E_n are the released energies of the alpha particle and neutron, respectively. In plasma heating, the alpha particles merely contribute and due to the plasma transparency, energetic neutrons escape freely. The neutrons energy deposition would be important, if the areal density of $(\rho\mathrm{R})_{n14} = 4.67$ g cm^{-2} for DT fuel is maintained. Therefore, their contribution in energy deposition is neglected freely in the calculations. Practically, a fraction of alpha energy is deposited in the fuel (f_α) depending on the areal density of igniting plasma; in this way, $(1 - f_\alpha)$ is the fraction of energy which is transferred into the outer cold fuel or tamper layers. f_α cannot be calculated analytically for cylindrical geometry unlike the spherical fuel volumes; hence, the approximate formula for the fraction of alpha energy deposition due to coulomb collision with plasma electrons in the fuel for a magnetized DT cylinder of radius, R, with a uniform magnetic field along the cylinder axis is presented by [29].

$$f_\alpha(x_\alpha) = \frac{x_\alpha + x_\alpha^2}{1 + 13x_\alpha/9 + x_\alpha^2} \tag{4}$$

with x_a,

$$x_\alpha(\bar{R}, b) = \frac{8}{3}\left(\bar{R} + \frac{b^2}{\sqrt{9b^2 + 1000}}\right), \tag{5}$$

which is a function of two dimensionless parameters, $\bar{R}$ and b,

$$\bar{R} = \frac{R}{l_\alpha}, \tag{6}$$

where R(cm) is the radius of cylindrical fuel volume. l_α(-cm) is the mean free path of alpha particles which is defined as [32, 42]:

$$l_\alpha[\mathrm{cm}] = \frac{3}{4\sqrt{2\pi}} \frac{m_\alpha v_0 (k_\mathrm{B} T)^{3/2}}{7 Z_\alpha^2 e^4 n \sqrt{m_\mathrm{e}}} = 0.015 T_\mathrm{keV}^{3/2}/\rho. \tag{7}$$

Equation (6) represents the effectiveness of alpha particles energy deposition, geometrically. Moreover, the parameter b depicts the relative importance of enhanced alpha particle heating in magnetized fuel, as well as:

$$b = \frac{R}{r_{\alpha\mathrm{L}}}, \tag{8}$$

where $r_{\alpha\mathrm{L}}[\mathrm{cm}] = v_0/\omega_\alpha = v_0 m_\alpha c/(2eB)$ is the Larmor radius of alpha particles and BR is in unit of G cm [32].

2.1 Energy balance condition in a non-equilibrium plasma

For simplicity, it is assumed that the volume is a uniform cylinder of radius, R, which consists of a metallic tube filled with fuel plasma. A seed magnetic field is applied externally along the cylinder axis. The driving ion beam heats the outer part of the cylinder; it causes the expansion of the cylinder radially and hence drives the inner part of the tube toward the axis. A typical radius of the cylinders is approximately 1–3 mm [29]. The particles are ablated radially as the ignition occurs. The role of the magnetic field is to control alpha particles radial flux and inhibit heat conduction of electrons. This determines the framework in which the zero-dimensional equations can be solved if a sector of the cylinder is to be observed. Cylindrical geometry requirements, such as fuel mass and fraction of deposited energy by alpha particles, must be fulfilled at a zero-dimensional approach. Furthermore, it is also assumed that the steady-state approach is valid during the stagnation period lasting about 10^{-7}–10^{-8} s where the hydrodynamics expansion can be neglected [42]. The ignition criterion using the energy balance equation for DT targets is primarily evaluated. The balance equation is written for cylindrical volumes surrounded by a tamper at the time of maximum compression (stagnation). Generally, the steady-state equation which refers to power balance as well as ignition criterion including essential physical processes will be determined by the following equation for stagnation, when temperature variation rate is almost zero.

$$W_\alpha - \sum W(\mathrm{losses}) \geq 0, \tag{9}$$

where W (gains) refers to all plasma heating mechanisms, specifically, alpha particles here. The second term in Eq. (9) includes the cooling processes by Bremsstrahlung radiation as well as plasma thermal conductions. Therefore, each term in Eq. (9) will take the following expressions assuming the equimolar DT with equal number densities ($n = n_\mathrm{e} = n_\mathrm{i}$):

$$W_\alpha\left[\frac{\mathrm{erg}}{\mathrm{cm}^3 \cdot \mathrm{s}}\right] = n_\mathrm{D} n_\mathrm{T} \langle \sigma v \rangle_\mathrm{DT} E_\alpha, \tag{10}$$

where W_α shows the energy deposition by alpha particles and $\langle \sigma v \rangle_\mathrm{DT}$ is the averaged Maxwellian reactivity of DT over 1 keV $< T_\mathrm{i} <$ 100 keV [43]. Ignition will never occur if losses due to conduction and radiation are too large. According to this, the fuel will burn efficiently provided that the deposition energy of thermonuclear alpha particles exceeds loss terms. Heating by alpha particles is the most important term in the power balance at stagnation. Moreover, with the addition of a magnetic field, alpha particles follow helical paths. As a result, the fraction of alpha particle energy deposited in the fuel increases. It has been shown that in magnetized fuel, alpha particles cause a significant ρR reduction, so that their Larmor radius is smaller than the DT cylinder radius ($R \ll l_\alpha$) [42]. Bremsstrahlung power density and heat conduction loss can be obtained by [29, 44]:

$$W_\mathrm{br}\left[\frac{\mathrm{erg}}{\mathrm{cm}^3 \cdot \mathrm{s}}\right] = \frac{16\pi^2}{3^{1/2}} \cdot \frac{(k_\mathrm{B} T_\mathrm{e})^{1/2} e^6}{m_\mathrm{e}^{3/2} c^3 h} n_\mathrm{e} \sum (n_\mathrm{i} Z^2), \tag{11}$$

$$W_\mathrm{hc}\left[\frac{\mathrm{erg}}{\mathrm{cm}^3 \cdot \mathrm{s}}\right] = \frac{2k_\mathrm{B}(\kappa_\mathrm{e} T_\mathrm{e} + \kappa_\mathrm{i} T_\mathrm{i})}{R^2}, \tag{12}$$

where κ_i and κ_e are Braginskii heat conduction coefficients [41]. Magnetic field enters into the balance equation through these coefficients which include the aforementioned cyclotron frequency of particles and also f_α. On this account, Eq. (9) simply changes into the following at stagnation:

$$W_\alpha - W_\mathrm{br} - W_\mathrm{hc} \geq 0. \tag{13}$$

We can assume either a spherical or cylindrical target containing a DT fuel. For cylindrical implosion with uniform fuel density, substitution of Eqs. 10–12 into Eq. (13) gives us the final expression including ρ, R, T_i, T_e, and

B parameters. Hence, the impact of the seed magnetic field can be described by various kinds of diagrams known as Lindl–Widner diagrams relating ρR and T parameters to each other [1].

2.2 Non-equilibrium ignition criterion in MTF

Ignition criterion for standard ICF in equilibrium mode is normally presented as a function of temperature and areal density [32]. However, there will be a distinct result for this criterion in the presence of magnetic field. This criterion has been particularly evaluated for magnetized case in equilibrium mode in other studies [29, 42]. A non-equilibrium mode of ignition criterion for magnetized DT fuel in cylindrical geometry is suggested in this paper. Therefore, taking into account the calculations in Ref. [29] at stagnation, the most prominent condition to be fulfilled is that the deposition of alpha particles exceeds Bremsstrahlung radiation ($W_{\alpha} > W_{br}$), and Eqs. (10) and (12) imply that

$$f_{\alpha} > 3.8 \times 10^{-18} \frac{T_e^{1/2}[\mathrm{keV}]}{\langle \sigma v \rangle_{DT}}. \tag{14}$$

If we add heat conduction as a second term for cooling, i.e., $W_{\alpha} > W_{br} + W_{hc}$, we will arrive at a general inequality for f_{α} and consequently for BR independent of ρ.

$$f_{\alpha} > 1.22 \times 10^{-41} \frac{\left(\frac{1.15 \times 10^{24} T_i^{1/2}[\mathrm{keV}]}{b^2} + 3.11 \times 10^{23} T_e^{1/2}[\mathrm{keV}] \right)}{\langle \sigma v \rangle_{DT}} \tag{15}$$

By substitution of the approximate value of f_{α} into Eq. (15), the ignition criterion for DT magnetized fuel in non-equilibrium mode will be obtained, which is an extensive statement based on T_e and T_i. For the special case of $T_i = T_e = T$, $BR \geq (6.13–4.64) \times 10^5$ G cm will be achieved that is in good agreement with Basko's calculations for equilibrium case (T =7–10 keV) [32].

3 Results and discussion

3.1 Lindl–Widner diagrams

The Lindl–Widner (LW) diagrams can explain the relation among T_i, T_e, and ρR in order to analyze ignition conditions. The form of curves in these diagrams in our study differs from non-magnetized as well as from the equilibrium case owing to an additional B parameter and the variation between electron and ion temperatures. Regarding calculations of balance equation, it is apparent that ion temperature just presents itself in $<\sigma v>_{DT}$ which is a function of ion temperature, T_i [45]. As a result, the higher ion temperature can give rise to a fusion reaction rate. Since the fraction of alpha particle energy deposition (f_{α}) occurs due to collisions with plasma electrons, this fraction depends on ρR and T_e [46]. On the other hand, the energy of plasma will reduce by the powers of 7/2 and 1/2 proportional to ion and electron temperatures as a result of heat conduction and Bremsstrahlung losses, respectively. This shows that low electron temperature will greatly reduce losses. A variety of diagrams can be demonstrated along with various ignition parameters on account of applying an axial magnetic field. LW diagrams can display ignition parameters as a function of electron and ion temperature with the same ρR for each curve. Focusing attention on solving steady-state non-equilibrium equations, B/ρ (G cm^3 g^{-1}), mB (G cm g^{-1}), and BR (G cm) are selected as three free parameters for Figs. 1, 2, and 3. The reason why these free parameters are selected is discussed in the following part.

The ignition curve parameter in Fig. 1 is opted as B/ρ. Selecting this parameter is a reasonable choice in the presence of magnetic field, in line with the dependence of Braginskii formulas to B/ρ for electron and ion heat conduction coefficients. As B/ρ grows, ρR decreases for different values of T_i and T_e. Besides, the difference between ion and electron temperature is noticeable in smaller ρR so that the greatest difference is for $B/\rho = 10^8$ G cm^3 g^{-1}. Yet, from $B/\rho = 10^7$ G cm^3 g^{-1}, the magnetic field will only impact on further reduction of ion and electron temperatures. The parameter B/ρ is desirable because it is a constant of motion for quasi-adiabatic implosions which is conserved in the process of cylindrical implosions [29]. As the ratio of B/ρ approaches infinity, the required ρR for ignition tends to zero [32]. Variation of ρ and R along with the magnitude of magnetic field will affect the hot spot pressure. The larger the radius, the lower the hot spot pressure, which results in reducing requirements on capsule drive. By lowering the pressure, the required ρ decreases and reduces requirements on fuel assembly. For instance, in MagLIF experiment, by reducing ρR from 0.3 to 0.01 g cm^{-2}, the required pressure would decrease by a factor of 30 [47].

Combining the expression for the fuel mass ($m = \pi \rho R^2$) with the non-equilibrium equations, we find a new free parameter, mB (G cm g^{-1}). Therefore, in Fig. 2 corresponding to this parameter, the growth of mB will also reduce ρR confinement parameter gradually. Given that $mB \propto R^2$, this reduction rate is not comparable to that of the B/ρ parameter. Thus, assuming there is a need for low variation of ρR, magnetic field changes can be introduced into the product of mB. This shows that ignition ρR depends on the fuel mass at stagnation.

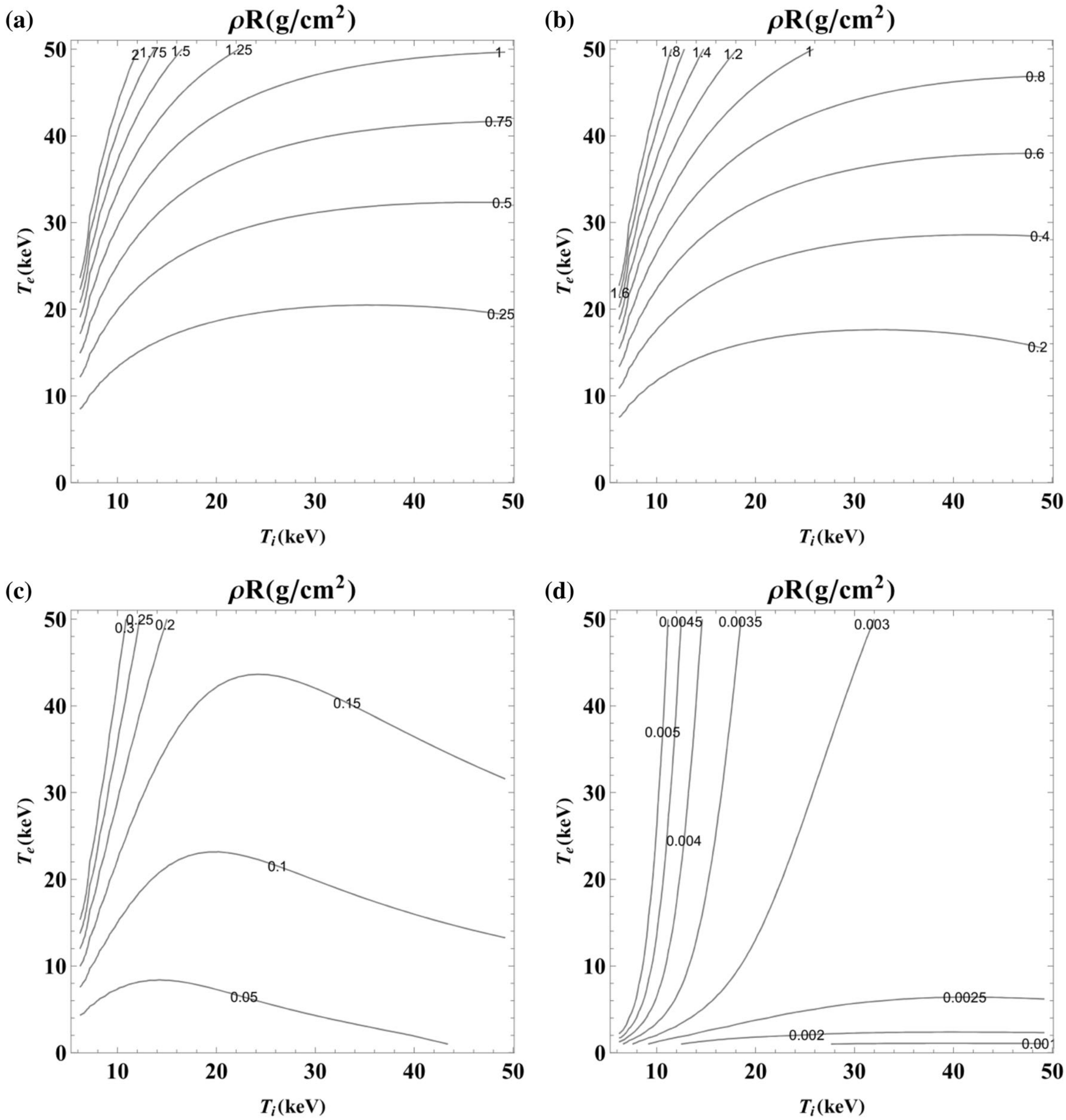

Fig. 1 Contours of ρR as a function of electron and ion temperatures for a fixed B/ρ parameter. **a** $B/\rho = 0$, **b** $B/\rho = 10^4$ G cm^3/g, **c** $B/\rho = 10^6$ G cm^3/g, and **d** $B/\rho = 10^8$ G cm^3/g

Since the typical ignition threshold is replaced with BR parameter or its equivalent parameter, $R/r_{\alpha L}$, this can be an appropriate criterion to discuss ignition conditions. As determined by Fig. 3, BR growth will also decrease ρR value. It is to be noted that from $BR = 4 \times 10^5$ G cm, MTF ignition domain will be valid for any ρR values. Once $B = 0$, all the three-parameter curves will behave in the same manner. Various other curves can be reproduced by multiplication of B/ρ into any power combination of T and ρR. It should be mentioned that synchrotron radiation loss is not entered in the computations. It has been proven that this radiation loss is negligible in analyzing magnetized ICF targets [48]. Comparing these curves with contour plots of ignition criterion for non-magnetized DT fuel as the one evaluated by Ref. [35] confirms the meaningful decrease in the ρR parameter. These figures are plotted for $T_{\mathrm{i}} > 6.0$ keV and $T_{\mathrm{e}} > 1.0$ keV. For the range of $6.0\ \mathrm{keV} < T_{\mathrm{i}} < 50.0\ \mathrm{keV}$ and $1.0\ \mathrm{keV} < T_{\mathrm{e}} < 50.0\ \mathrm{keV}$, ρR will vary from 0.002–2.0 g cm^{-2} intervals. For non-magnetized DT, we have $2.0\ \mathrm{g\ cm^{-2}} < \rho R < 0.1\ \mathrm{g\ cm^{-2}}$. These results are summarized in Table 1 for three known free parameters. For MagLIF at Sandia National Labora-

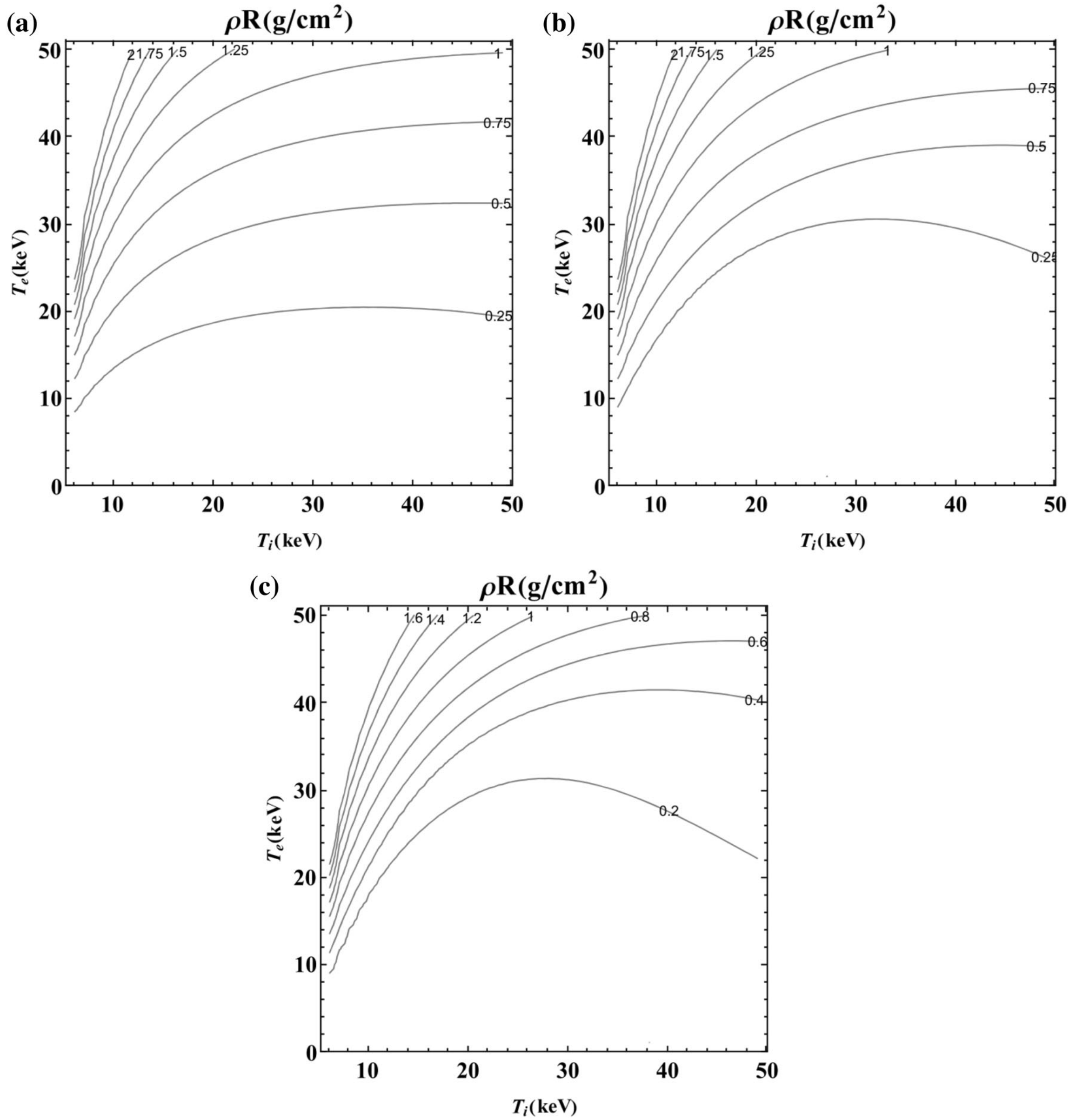

Fig. 2 Contours of ρR as a function of electron and ion temperatures for a fixed mB parameter. **a** $mB = 0$, **b** $mB = 2 \times 10^4$ G cm/g, **c** $mB = 3 \times 10^4$ G cm/g

tory, the magnetization parameter BR is 0.34 MG cm. BR, rather than ρ, is the fundamental confinement parameter relevant to MagLIF since it is related to the size [11]. For cylindrical targets with axial magnetic field, the extremely high BR appears at low densities. The other types of targets do not have such high BR at low density.

As we organize the balance equation based on B/ρ parameter, it implies that by increasing this parameter, heat conduction declines considering it is greatest power in the denominator of heat conduction term. This power is related to the dimensionless parameter of $\omega\tau$, the product of cyclotron frequency and collision time, which is recognized as magnetization term and shows the effect of magnetic field on transport coefficients [24, 30]. Magnetic field has no influence on Bremsstrahlung radiation power (see Eq. (11)). Enhancing B/ρ broadens ρR range along with lowering its value.

3.2 Calculation of ignition conditions for equilibrium case

Ignition criterion for magnetized DT fuel was formerly computed by Kemp [38]. In this section, the equilibrium case for steady state is discussed as a means to have a better perspective on non-equilibrium figures. If we invoke our calculations for this case, the fraction of energy deposited by alpha particles in Eq. (14) for $T_{\rm i} = T_{\rm e}$ and

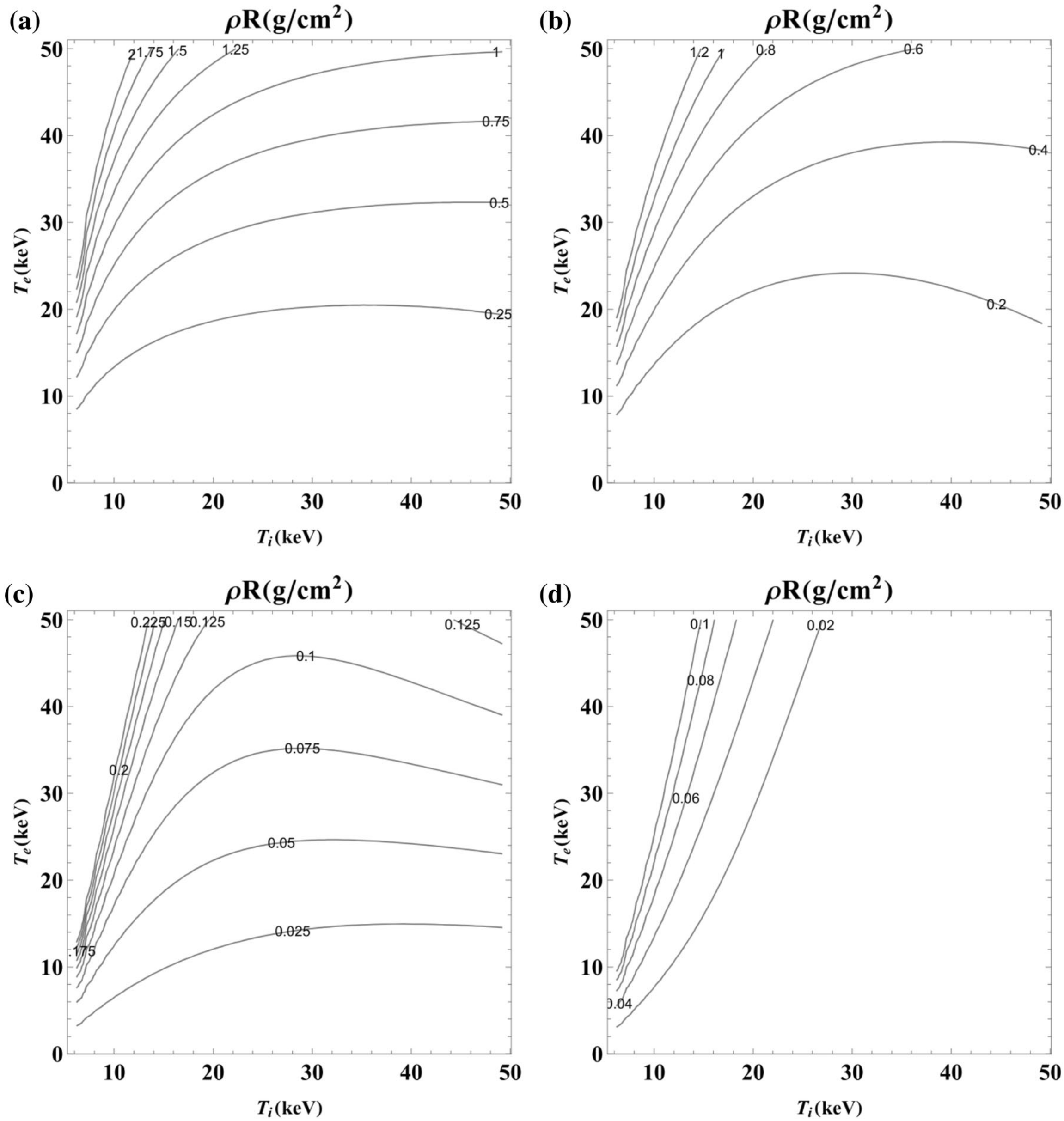

Fig. 3 Contours of ρR as a function of electron and ion temperatures for a fixed BR parameter. **a** $BR = 0$, **b** $BR = 0.2 \times 10^5$ G cm, **c** $BR = 2.2 \times 10^5$ G cm, and **d** $BR = 3 \times 10^5$ G cm

Table 1 Alternative ρR for three ignition parameters in magnetized DT fuel

BR (G cm)	ρR (g cm^{-2})	mB (G cm g^{-1})	ρR (g cm^{-2})	B/ρ (G cm^3 g^{-1})	ρR (g cm^{-2})
0.2×10^5	0.2–1.2	2.0×10^4	0.25–2.00	10^4	0.20–1.80
1.0×10^5	0.1–0.4	3.0×10^4	0.2–1.00	10^6	0.05–0.30
2.2×10^5	0.025–0.20	4.0×10^4	0.2–1.00	10^8	0.002–0.004
3×10^5	0.02–0.1.00				

$W_\alpha > W_{\mathrm{br}}$ will be summarized to $f_\alpha > 0.240$–0.105. Subsequently, $b > 1.73$–1.14 will be attained. Addition of heat conduction term to our inequality will yield $b > 2.27$–1.72. The derived ignition condition for magnetized cylindrical DT target is consistent with Kemp's criterion as follows:

$$BR \geq (6.13 - 4.64) \times 10^5 \ \mathrm{G \cdot cm}. \tag{16}$$

This limit is the condition of ignition to occur in DT cylindrical magnetized targets. Ignition boundaries can be calculated for the steady state from Eq. (9), similarly to the non-equilibrium case. If the ignition is achieved in the implosion process, the minimum of ρRT product will determine optimum entry point [30]. Referring to the magnetic field magnitude, this point is in the range of T = 6–8 keV based on our calculations. Figure 4 shows a tangible description.

To characterize the effect of growth in alpha particle energy deposition and reduction in heat conduction loss, other appropriate figures with various ignition parameters can be illustrated. B/ρ is analyzed, for instance, in Fig. 5. Remarkably, different criterions will be attained supposing that we suppress electron and ion heat conduction completely ($W_{hc} = 0$) or have local alpha particle energy deposition ($f_\alpha = 1$). Comparison of Fig. 5 with its counterpart in Ref. [29] clearly displays this difference. Eliminating heat conduction reduces constraint on ρR to a large extent to broaden its range. This range is even wider for $f_\alpha = 1$ and ρR reduces by about one order of magnitude.

4 Conclusion

Achieving ignition for inertial fusion based magnetized target has consistently been a concern for the last years. It is also considered as a smooth pathway to reach ignition criterion with lower fuel areal density (ρR). If this issue is analyzed by a non-equilibrium ignition model, it will be more attractive since temperature imbalance between ions and electrons is a factor yielding a lower limit for ρR with reduction of electrons and ions heat conduction and driver requirements in addition to the presence of an axial magnetic field. In this paper, ignition criterion for magnetized cylindrical hot plasma in the presence of an axial magnetic field is investigated using a non-equilibrium model. This criterion is calculated for pre-compressed DT plasma. The inequality between electrons and ions temperature is valuable so that it can smooth the ignition conditions in MTF. Ignition criterion is derived from solving the equation of energy balance within heating and cooling terms. It is described through parameter space formed from electron and ion temperature, plasma areal density, and any of

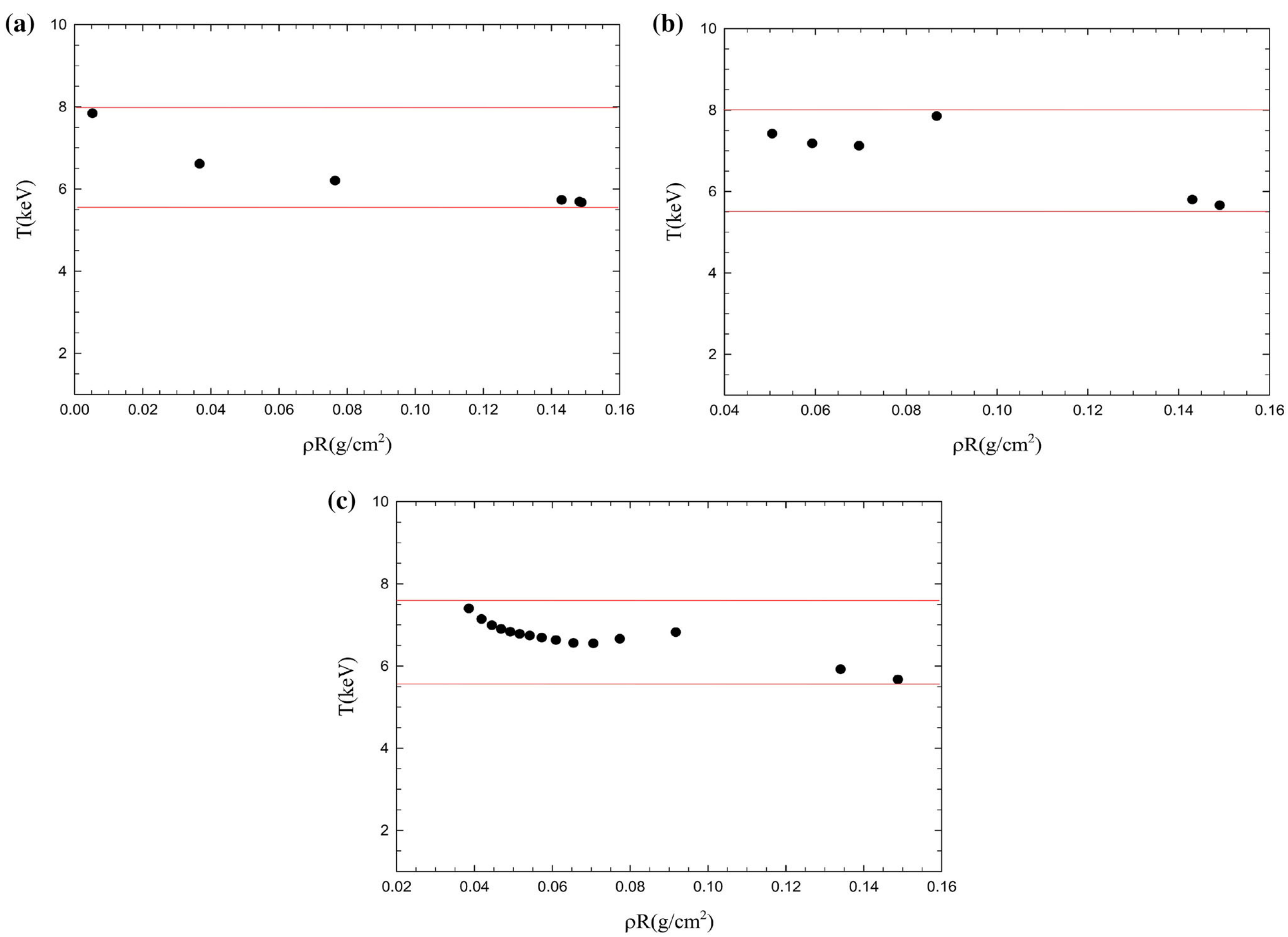

Fig. 4 Minimum allowed ρRT product for different free parameters **a** B/ρ, **b** *mB,* and **c** *BR*

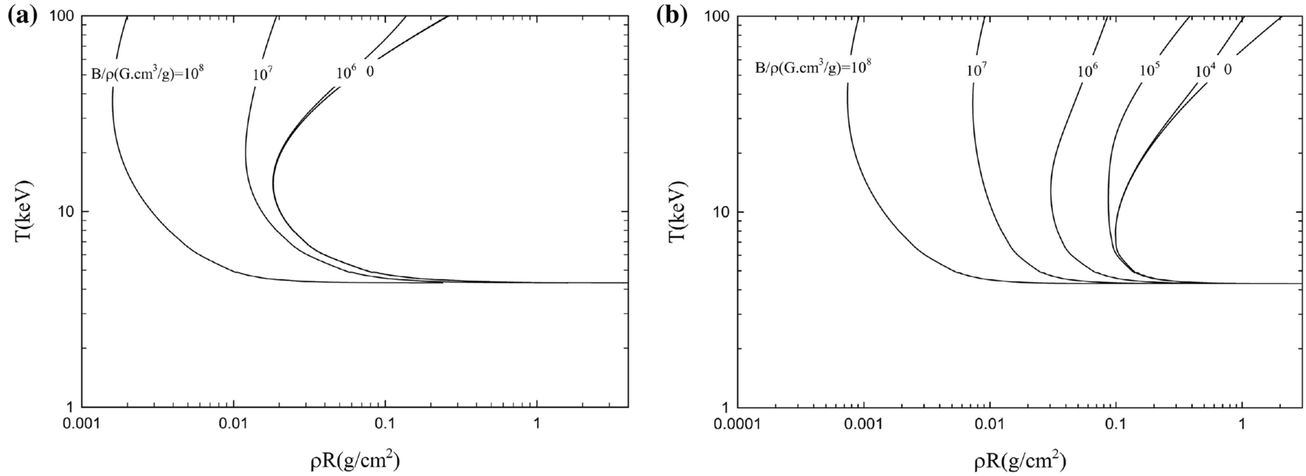

Fig. 5 ρRT diagram of cylindrical DT magnetized fuel for **a** $W_{hc} = 0$ and **b** $f_\alpha = 1$

ignition parameters owing to exertion of magnetic field, i.e., B/ρ, mB, or BR. Electron and ion temperature inequality combined with the impact of the axial magnetic field on reduction of electron and ion heat conduction loss and the enhancement of alpha particles energy deposition in comparison with the non-magnetized case will relax the conditions in which the ignition can occur. Moreover, there will be a significant decrease in ρR relative to the equilibrium case. The temperature difference is more notable in small ρRs, and it reaches its maximum value at $B/\rho = 10^8$ G cm^3 g^{-1}. Additionally, MTF range expands over all ρR values from $BR = 4 \times 10^5$ G cm.

Besides, we have done the calculations of ignition hydrodynamics for the steady state in equilibrium plasma, with the objective to verify the two-temperature magnetized model. The results of these calculations conform to two-temperature calculations. In order to further explore this model, other fuels can be evaluated and compared with the one-temperature model. The assumption of $T_i = T_e$ may not provide ignition condition for some fuels. Among the two main common ongoing classes of MTF, which are named as high gain and low-to-intermediate gain, our study best fits the first approach experiments. This is because the first approach consists of cryogenic targets, lowers the implosion velocity, and relaxes many design constraints increasing energy gain. Experiments at the University of Rochester are concerned with this approach using the OMEGA laser facility. This can also be done with multi-dimensional codes. Cylindrical liners in the MagLIF experiment, which are driven by an azimuthal or axial magnetic field, are also good examples of theoretical calculations.

References

1. R.C. Kirkpatrick, I.R. Lindemuth, M.S. Ward, Magnetized target fusion: an overview. Fusion Technol. **27**(3), 201–214 (1995). https://doi.org/10.13182/FST95-A30382
2. C. Yamanaka, Inertial confinement fusion: the quest for ignition and energy gain using indirect drive. Nucl. Fusion **39**, 825 (1999). https://doi.org/10.1088/0029-5515/39/6/702
3. S. Atzeni, J. Meyer-ter-Vehn, *The Physics of Inertial Fusion: BeamPlasma Interaction, Hydrodynamics, Hot Dense Matter* (Oxford University Press, New York, 2004), pp. 35–39
4. R.C. Kirkpatrick, HEDP and new directions for fusion energy. High Energy Density Phys. **6**, 207–209 (2010). https://doi.org/10.1016/j.hedp.2010.01.017
5. I.R. Lindemuth, An extended study of the ignition design space of magnetized target fusion. Phys. Plasmas **24**, 055602 (2017). https://doi.org/10.1063/1.4977538
6. I.R. Lindemuth, R.E. Siemon, The fundamental parameter space of controlled thermonuclear fusion. Am. J. Phys. **77**, 407–416 (2009). https://doi.org/10.1119/1.3096646
7. M. Sweeney, A. Farnsworth Jr., High-gain, low-intensity ICF targets for a charged-particle beam fusion driver. Nucl. Fusion **21**, 41 (1981). https://doi.org/10.1088/0029-5515/21/1/004
8. I. Lindemuth, R. Kirkpatrick, Parameter space for magnetized fuel targets in inertial confinement fusion. Nucl. Fusion **23**, 263 (1983). https://doi.org/10.1088/0029-5515/23/3/001
9. I. Lindemuth, R. Reinovsky, R. Chrien, et al., Joint US/Russian plasma formation experiments for magnetic compression/magnetized target fusion (MAGO/MTF), in *Digest of Technical Papers. Tenth IEEE International Pulsed Power Conference, Albuquerque, NM, USA*, vol. 1 (1995), pp. 601–606. https://doi.org/10.1109/ppc.1995.596738
10. A.B. Sefkow, S. Slutz, J. Koning et al., Design of magnetized liner inertial fusion experiments using the *Z* facility. Phys. Plasmas **21**, 072711 (2014). https://doi.org/10.1063/1.4890298
11. K. Hahn, G.A. Chandler, C.L. Ruiz et al., Fusion-neutron measurements for magnetized liner inertial fusion experiments on the Z accelerator. J. Phys: Conf. Ser. **717**, 012020 (2016). https://doi.org/10.1088/1742-6596/717/1/012020
12. A. Kemp, M. Basko, J. Meyer-ter-Vehn, Magnetized cylindrical targets for heavy ion fusion. Nucl. Instrum. Methods Phys. Res. Sect. A **464**, 192–195 (2001). https://doi.org/10.1016/s0168-9002(01)00032-8

13. D. Kilcrease, R. Kirkpatrick, Magnetized fuel inertial confinement fusion. Nucl. Fusion **28**, 1465 (1988). https://doi.org/10.1088/0029-5515/28/8/015
14. A.J. Kemp, M.M. Basko, J. Meyer-ter-Vehn, Implosion and ignition of magnetized cylindrical targets driven by heavy-ion beams. Nucl. Fusion **43**, 16 (2002). https://doi.org/10.1088/0029-5515/43/1/302
15. I.R. Lindemuth, The ignition design space of magnetized target fusion. Phys. Plasmas **22**, 122712 (2015). https://doi.org/10.1063/1.4937371
16. R. Ramis, J. Meyer-Ter-Vehn, On thermonuclear burn propagation in a pre-compressed cylindrical DT target ignited by a heavy ion beam pulse. Laser Part. Beams **32**, 41–47 (2014). https://doi.org/10.1017/S0263034613000839
17. M. Basko, M. Churazov, A. Aksenov, Prospects of heavy ion fusion in cylindrical geometry. Laser Part. Beams **20**, 411–414 (2002). https://doi.org/10.1017/S0263034602203080
18. M. Widner, J. Chang, A. Farnsworth et al., Neutron-production from relativistic electron-beam targets. in *Bulletin of the American Physical Society, American Institute of Physics Circulation and Fulfillment Division, 500 Sunnyside Blvd, Woodbury, NY 11797–2999* (1977), pp. 1139–1139. https://doi.org/10.1111/j.1749-6632.1975.tb00096.x
19. R. Jones, W. Mead, The physics of burn in magnetized deuterium-tritium plasmas: spherical geometry. Nucl. Fusion **26**, 127 (1986). https://doi.org/10.1088/0029-5515/26/2/001
20. S.A. Slutz, R.A. Vesey, High-gain magnetized inertial fusion. Phys. Rev. Lett. **108**, 025003 (2012). https://doi.org/10.1103/PhysRevLett.108.025003
21. P. Schmit, P. Knapp, S. Hansen et al., Understanding fuel magnetization and mix using secondary nuclear reactions in magneto-inertial fusion. Phys. Rev. Lett. **113**(15), 155004 (2014). https://doi.org/10.1103/PhysRevLett.113.155004
22. K. Schoenberg, R. Siemon, Magnetized target fusion, in *A Proof-of-Principle Research Proposal* (Los Alamos National Lab, NM, US, 1998). https://doi.org/10.2172/763201
23. G.A. Wurden, S.C. Hsu, T.P. Intrator et al., Magneto-inertial fusion. J. Fusion Energy **35**, 69–77 (2016). https://doi.org/10.1007/s10894-015-0038-x
24. S.C. Hsu, S.J. Langendorf, Magnetized plasma target for plasma-jet-driven magneto-inertial fusion. J. Fusion Energy **38**, 182–198 (2018). https://doi.org/10.1007/s10894-018-0168-z
25. J. Davies, R. Betti, P.Y. Chang et al., The importance of electrothermal terms in Ohm's law for magnetized spherical implosions. Phys. Plasmas **22**, 112703 (2015). https://doi.org/10.1088/0029-5515/43/1/302
26. M. Basko, Magnetized implosions driven by intense ion beams. Phys. Plasmas **7**, 4579–4589 (2000). https://doi.org/10.1063/1.1312182
27. M. Basko, J. Maruhn, T. Schlegel, Hydrodynamic instability of shells accelerated by direct ion beam heating. Phys. Plasmas **9**, 1348–1356 (2002). https://doi.org/10.1063/1.1462634
28. A. Kemp, M. Basko, J. Meyer-ter-Vehn, Ignition conditions for magnetically insulated tamped ICF targets in cylindrical geometry. Nucl. Fusion **41**, 235 (2001). https://doi.org/10.1088/0029-5515/41/2/311
29. A.J. Kemp, *Magnetized Cylindrical Implosions Driven by Heavy ion Beams*. Ph.D. Thesis, Technische Universität München (2001)
30. T. Intrator, S.Y. Zhang, J.H. Degnan et al., A high density field reversed configuration (FRC) target for magnetized target fusion: first internal profile measurements of a high density FRC. Phys. Plasmas **11**, 2580–2585 (2004). https://doi.org/10.1063/1.1689666
31. I. Lindemuth, R. Kirkpatrick, The promise of magnetized fuel: inertial confinement fusion with existing driver technology. Atomkernenerg/Kerntech **45**, 9–13 (1984)
32. M. Basko, A. Kemp, J. Meyer-ter-Vehn, Ignition conditions for magnetized target fusion in cylindrical geometry. Nucl. Fusion **40**, 59 (2000). https://doi.org/10.1088/0029-5515/41/2/311
33. M. Temporal, A. Piriz, N. Grandjouan et al., Numerical analysis of a multilayered cylindrical target compression driven by a rotating intense heavy ion beam. Laser Part. Beams **21**, 609–614 (2003). https://doi.org/10.1017/S0263034603214208
34. O.V. Gotchev, N.W. Jang, J.P. Knauer et al., Magneto-inertial approach to direct-drive laser fusion. J. Fusion Energy **27**, 25–31 (2008). https://doi.org/10.1007/s10894-007-9112-3
35. S. Eliezer, Z. Henis, N. Nissim et al., Introducing a two temperature plasma ignition in inertial confined targets under the effect of relativistic shock waves: the case of DT and pB 11. Laser Part. Beams **33**, 577–589 (2015). https://doi.org/10.1017/S0263034615000701
36. Z. Fan, J. Liu, B. Liu et al., Ignition conditions relaxation for central hot-spot ignition with an ion-electron non-equilibrium model. Phys. Plasmas **23**, 010703 (2016). https://doi.org/10.1063/1.4940315
37. Z. Fan, Y. Liu, B. Liu et al., Non-equilibrium between ions and electrons inside hot spots from National Ignition Facility experiments. Matter Radiat. Extremes **2**, 3–8 (2017). https://doi.org/10.1016/j.mre.2016.11.003
38. J.W. Li, L. Chang, Y.S. Li et al., Transition from equilibrium ignition to non-equilibrium burn for ICF capsules surrounded by a high-*Z* pusher. Nucl. Fusion **51**, 063005 (2011). https://doi.org/10.1088/0029-5515/51/6/063005
39. Z. Fan, X. He, J. Liu et al., A wedged-peak-pulse design with medium fuel adiabat for indirect-drive fusion. Phys. Plasmas **21**, 100705 (2014). https://doi.org/10.1063/1.4898682
40. F.F. Chen, S.E. Von Goeler, *Introduction to Plasma Physics and Controlled Fusion Volume 1: Plasma Physics* (Springer, Berlin, 1983), pp. 6–7
41. S. Braginskii, *Transport Processes in a Plasma, Consultants Bureau* (New York, 1965), pp. 215–249
42. C. Cereceda, C. Deutsch, M. De Peretti et al., Kinetic theory of alpha particles production in a dense and strongly magnetized plasma. Phys. Plasmas **7**, 4515–4533 (2000). https://doi.org/10.1063/1.1308564
43. H.-S. Bosch, G. Hale, Improved formulas for fusion cross-sections and thermal reactivities. Nucl. Fusion **32**, 611 (1992). https://doi.org/10.1088/0029-5515/32/4/I07
44. B. Zohuri, *Inertial Confinement Fusion Driven Thermonuclear Energy* (Springer, Cham, 2017), pp. 146–147
45. W.A. Fowler, G.R. Caughlan, B.A. Zimmerman, Thermonuclear reaction rates. Ann. Rev. Astron. Astrophys. **5**, 525–570 (1967). https://doi.org/10.1146/annurev.aa.05.090167.002521
46. R. Betti, A. Christopherson, B. Spears et al., Alpha heating and burning plasmas in inertial confinement fusion. Phys. Rev. Lett. **114**, 255003 (2015). https://doi.org/10.1088/1742-6596/717/1/012007
47. M.C. Hermann, M.E. Cuneo, D.B. Sinars et al., Magnetically driven implosions for inertial confinement fusion at Sandia National Laboratories. IEEE Trans. Plasma Sci. **40**, 3222–3245 (2012). https://doi.org/10.1109/tps.2012.2223488
48. M. Basko. Inertial confinement fusion with magnetized fuel in cylindrical targets, in *Rep. EURCEA-FC 1645, CEA Cadarache* (1998)